Pipeline for 3D reconstruction of lung surfaces using intrinsic features under pressure-controlled ventilation

Samuel Richardson[a], Thiranja P. Babarenda Gamage[a] , Toby Jackson[a], Amir HajiRassouliha[a], Alys Clark[a], Martyn P. Nash[a,b], Andrew Taberner[a,b], Merryn H. Tawhai[a], Poul M.F. Nielsen[a,b]

a Auckland Bioengineering Institute, University of Auckland, New Zealand
b Department of Engineering Science, University of Auckland, New Zealand

Abstract

The measurement of whole lung mechanics forms the basis of diagnostic measurements for many respiratory diseases. Despite this, there are currently no quantitative methods to link alterations in pulmonary microstructures to measurements of whole lung function. The normal decline in the lung's microstructure that occurs with age is virtually indistinguishable from early disease on imaging or standard lung function measurements, leading to frequent misdiagnosis in the elderly. Accurate characterisation of lung mechanics across spatial scales has the potential to assist distinguishing age from pathology, which would benefit patients across a range of medical conditions and procedures. While computational modelling promises to be a useful tool for improving our understanding of lung mechanics, there is currently no unified structure-function computational model that explains how age-dependent structural changes translate to decline in whole lung function. This paper presents novel instrumentation and imaging techniques for measurements of intact *ex vivo* lung tissue mechanics. We seek to address problems of weak parameterisation that existing models suffer from, due to lack of reliable measurements. To begin addressing this issue, we have developed a full-field stereoscopic imaging system for tracking surface deformation of the rat lung during pressure-controlled ventilation. This study presents a pipeline for the reconstruction and tracking of the intact left lobe of a rat lung during inflation, *ex vivo*. Model-based 3D reconstruction of the lungs enabled the 3D shape of a surface patch of the imaged lung to be determined. The 3D reconstruction and tracking of the fresh lung surface patch in this study was completed with three cameras across 21 pressure steps, encompassing a total pressure change from 2069 Pa to 2386 Pa. This approach shows that reconstructing intact *ex vivo* fresh lungs, with no additional surface markers, is feasible.

1. Introduction

Despite the importance of the lungs in delivering oxygen to the body, aspects of their mechanics remain poorly understood [1]. A key reason for this is that any disruption of the lung structure results in a change in the mechanical response of the tissue, making traditional mechanical testing poorly suited to investigating lung tissue [2]. Many studies have attempted to characterise the mechanics of lung tissues, however, it was not until the middle-to-late 20th century that respiratory mechanics began to be studied as a separate field, and it was during this time that the majority of our understanding was developed [3, 4]. Despite advances in imaging technologies, fundamental questions concerning key processes that occur in the lungs remain unanswered. For example, there is no unifying theory for alveolar dynamics and recruitment during respiration. It remains unclear if the alveoli expand isotropically, heterogeneously, or by a combination of both [5]. This has been debated in the literature, with consensus being hindered by difficulties in imaging the small and constantly moving alveoli during respiration.

Computational modelling may prove to be a useful tool for improving our understanding of lung mechanics, and several computational models have been proposed for the mechanics of lung tissue. However, there is currently no unified structure-function computational model that explains how age-dependent structural changes translate to decline in whole lung function. Existing models suffer from weak parameterisation due to lack of available data. In this study, we designed a real-time full field stereoscopic imaging system for tracking lung surface deformation under pressure-controlled inflation. This system will enable us to acquire rich, accurate, robust, and previously unavailable physiological data on lung tissue mechanics from whole rat lungs, that can ultimately be used to parameterise computational models of lung mechanics.

2. Methodology

2.1 Lung Ventilation

Fresh post-mortem lungs were acquired from female (350 ± 50) g Sprague-Dawley rats, after the animals were sacrificed following separate experimental studies that did not involve the chest cavity. The Sprague-Dawley strain was chosen for two key reasons: similarities to humans in alveolar air-space enlargement with age [6]; and their relatively large alveoli (~90 μm diameter) [6] compared with lung size (~20 mL). A cannulated rat lung is shown in Fig 1.

A CompactRio (National Instruments) based real time pressure control system was developed to control the inflation of the lungs. A syringe pump enabled real time pressure control, with volume and pressure resolutions of ±5 μl and ±5 Pa

respectively. A 100 ml glass syringe was mounted and actuated by a Physik Instrumente DC-Mike linear actuator that has an encoder resolution of 0.0592 µm.

During stereoscopic imaging of the lungs, images were captured at regular intervals corresponding to increments/decrements in pressure of 15 Pa. Fig 2 shows the pressure-volume (PV) loops from the stereoscopic measurement of the lung lobe. The imaged inflation cycle (red in Fig 2) shows three cycles between 2000 Pa and 3000 Pa. The PV loops between 2000 Pa and 3000 Pa are approximately linear, with a small amount of hysteresis visible between 2800 Pa and 3000 Pa. There was an increase in lung volume of 0.2 mL across the three loops, when comparing the volumes at 2000 Pa.

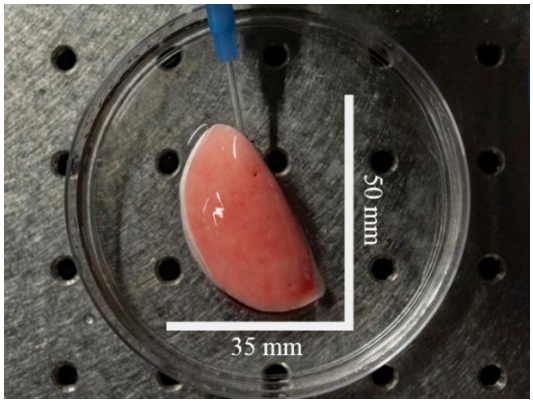

Fig 1. Inflated left lung lobe held at 3000 Pa, in a Petri dish full of phosphate buffered saline solution and cannulated with a plastic 16 Gauge blunted needle.

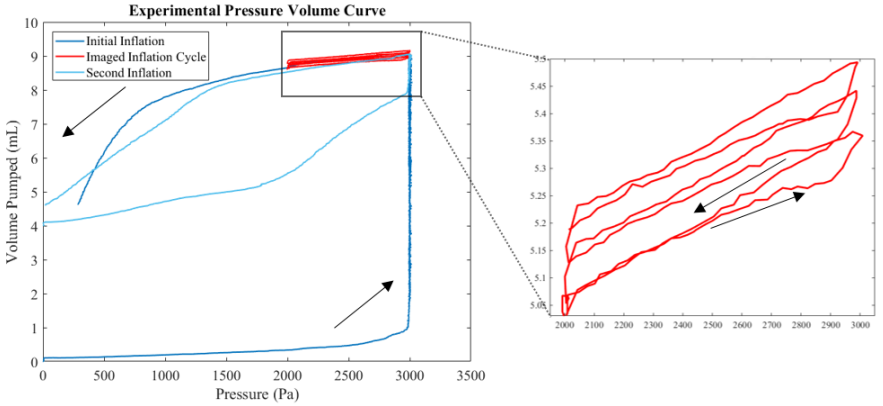

Fig 2. Left, PV loops from two full range inflations and an imaging cycle of three PV loops from 2000 Pa to 3000 Pa and back. Arrows depict the direction of increasing time. Right, expanded view of the three PV loops used for imaging.

2.2 Lung Surface Imaging

A 12 camera full field stereoscope was designed and built in-house to enable imaging of the surface displacement of the lung during pressure-controlled inflation. FLIR BlackflyS monochrome cameras that feature a SONY IMX250 sensor were selected for imaging the lung due to their high quantum efficiency and high signal to noise ratio (4760 signal to noise ratio or 73 dB dynamic range). The sensors had a 2448 pixel × 2048 pixel resolution (5.0 MP) with a 3.45 µm pixel size and were capable of imaging at 75 frames per second. The control code for these cameras was written in LabView (National Instruments), enabling data from all 12 cameras to be saved concurrently.

To ensure accurate 3D reconstruction of the imaged objects, the cameras were calibrated to find their intrinsic and extrinsic parameters, and the mounting of the cameras was designed for rigidity, to ensure that the cameras remain fixed relative to one another. The design and construction of this stereo system has been described previously for eight cameras [7]. Several modifications have been made since this was previously reported and are presented in the following sections.

2.2.2 Stereo Rig Construction

A rigid camera frame was designed in Solidworks. To ensure sufficient rigidity between the cameras, the geometry of the camera frame was designed as a regular octahedron, as shown in Fig 3. To ensure consistent lighting, eight high-power 1270 lm LED Engin LZ1-10R200 light emitting diodes were used with diffusers to ensure even lighting and to reduce noise in the camera images. Image acquisition from the cameras was performed in LabVIEW and the cameras were synchronized using a hardware trigger from the pressure control FPGA. This enabled images to be triggered, based on changes in pressure.

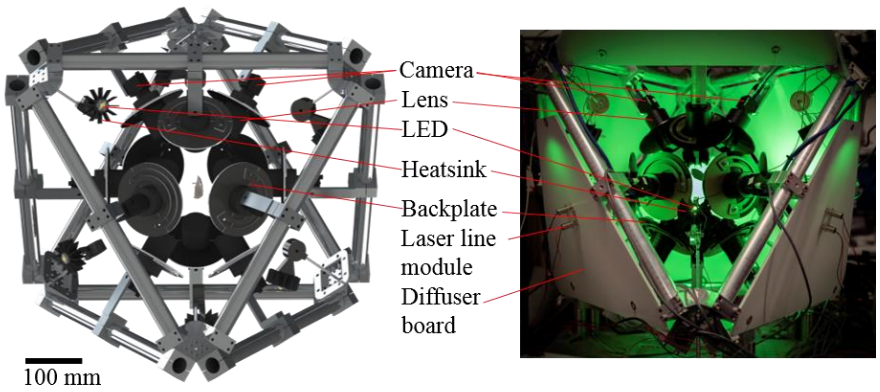

Fig 3. Frame constructed for performing full-field imaging of the lung surface during pressure-controlled inflation experiments. Left shows a CAD rendering of the stereo rig, Right shows the physical rig.

Lungs were dissected from the rats *en bloc*, with the heart and trachea attached. The heart and right lobes were removed, leaving the left lobe and a length of bronchus for cannulation. After cannulation of the lungs onto a blunted needle, they were attached to the syringe pump system. This enabled the initial inflation of the lungs from their collapsed state. The lungs were inflated to a pressure of 3000 Pa and held at that pressure until fully inflated. After a full inflation/deflation cycle, the lungs were bathed in phosphate buffered saline (PBS) to ensure that they remained hydrated. Post hydration, the lungs were mounted into the centre of the stereo camera system.

2.2.3 Stereo Rig Calibration

Camera calibration is necessary to achieve high accuracy imaging and 3D reconstruction. The accuracy of any 3D measurement made with a stereo imaging system depends, in part, on the accuracy of the calibration of the stereo cameras. The process of calibrating a camera system is a complex problem, which grows in complexity with every additional camera. The calibration method used in this study was developed by HajiRassouliha *et al* [8] using a checkerboard calibration template. This has been described by HajiRassouliha *et al* in [8] for cameras where all cameras could see the same calibration template. In this study, we extended the calibration approach to allow for calibration of all cameras in the stereo rig. This involved calibrating overlapping groups of four cameras, followed by an alignment of the calibrated cameras sets using a 3D triangular template with three white cellulose precision microspheres of a known diameter attached to each of its vertices. The diameters and spacing between spheres were identified using micro-CT imaging with a resolution of 2.7 μm.

2.2.4 Initial Surface Reconstruction

The first step in an inflation was to acquire images of the *ex vivo* lung while it was illuminated by a laser line, as depicted in Fig 4. Images including laser lines were acquired without LED illumination These data were used to generate an initial 3D reconstruction of the lung shape. This involved segmenting and fitting the laser lines on the lung lobe using piecewise cubic splines in each of the 2D images from each camera view. The pixel coordinates of these splines were triangulated into 3D space by determining their locations across multiple cameras using an intersecting ray approach, as described in [11], with the requirement that four rays intersect for a point to be considered valid. This resulted in a 3D point cloud which described the surface of the lung.

Immediately after laser line data acquisition, the lungs were cyclically inflated and deflated for imaging.

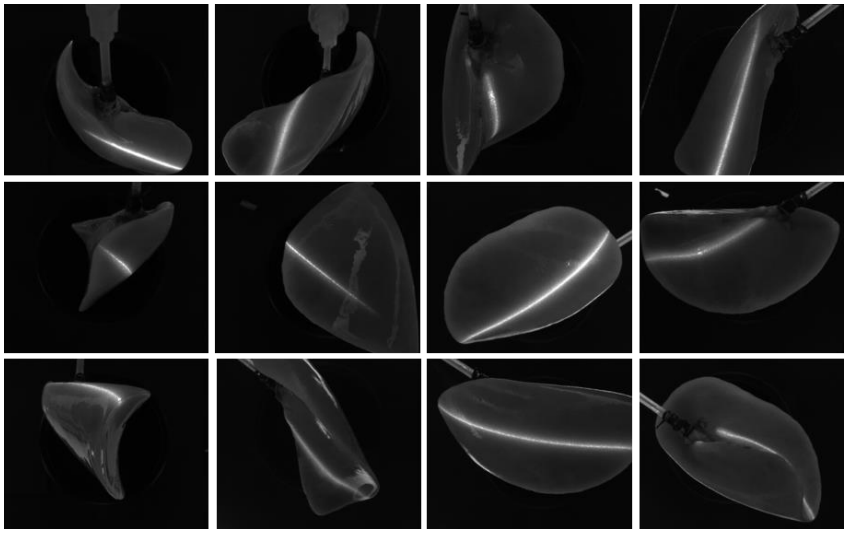

Fig 4. Examples of laser line images. The lungs were held at a fixed pressure while each line was acquired individually. In this data set, the lungs were held at 2000 Pa. Firstly, images of the lungs were taken at different levels of illuminations from LEDs, then 22 images were recorded of individual laser lines on the lungs.

2.3 Lung Fixing and Micro Computed Tomography (CT) Imaging

To obtain an initial estimate of the 3D shape of the lungs, after stereoscopic imaging, lungs were fixed and imaged using a Bruker SkyScan 1272, micro-CT scanner at a pixel resolution of 25 μm. The lungs were fixed by inflating the lungs with 2.5 % glutaraldehyde buffered with phosphate buffered saline solution, up to a pressure of 2450 Pa (25 cmH_2O). Tissue samples fixed in glutaraldehyde are extensively cross-linked, providing excellent ultrastructural stiffening that maintains the structure of the alveoli, enabling imaging with micro-CT [9]. This process was carried out after stereoscopic imaging, as cross-linking reactions of glutaraldehyde are largely irreversible [10].

The lungs were held at the fixation pressure for 24 h. After 24 h the lungs were attached to a regulated air source, which maintained an even pressure of 2450 Pa (25 cmH_2O) to air dry the fixed lungs. The result of this process was a dried lung lobe, with no living tissues, and with the structural proteins cross-linked to maintain the lung structures. An example of this can be seen in Fig 5.

The micro-CT image of the lung lobe, shown in Fig 5, enabled the creation of a mesh of the lung lobe. This process started with thresholding of the 2D images to create binary masks. Any holes in the masks were corrected manually. An ITK-based marching cubes algorithm was then implemented to convert each binary mask into a 3D isosurface, which was converted into a point cloud that represented the surface of the lungs from the micro-CT data. While some discrepancies were

introduced by the cross-linking procedure and shrinkage during the air-drying process, the mesh of the fixed lung generated from micro CT imaging provided a close approximation to the shape of the unfixed lung.

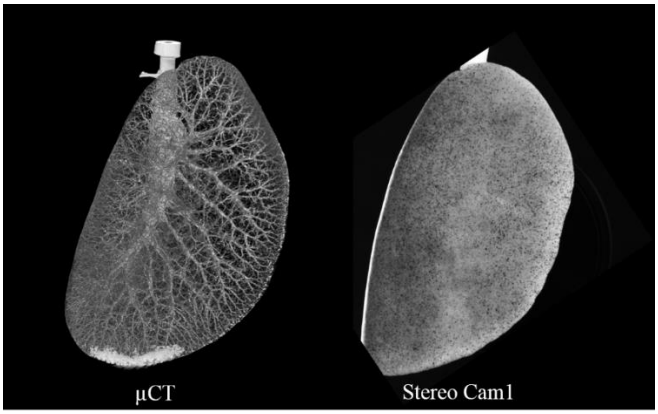

Fig 5. Left, Micro-CT of the fixed lung lobe. Right, view of fixed speckled lung from a single camera.

2.4 Improving Lung Surface Reconstruction and Tracking Motion

The dense point cloud created from the segmented micro-CT data described in Section 2.3 was aligned to the sparsely reconstructed laser line data acquired from the stereo rig described in Section 2.2.4 using a coherent point drift algorithm to rigidly translate, rotate, and scale the point cloud.

A quadratic Lagrange surface mesh was fitted to the aligned micro-CT point cloud using the fitting algorithms in GIAS2 [12], which minimises the weighted sum of the projections of the point cloud onto the surface. The result of this procedure was an initial surface mesh that was aligned with the position of the stereo-imaged lung, as shown in Fig 6.

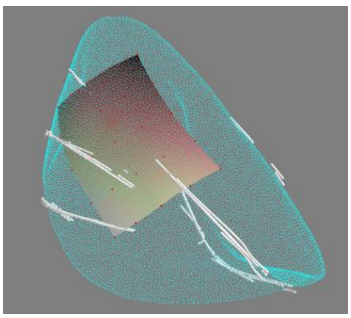

Fig 6. Fresh lung meshes. Laser line points are white. The micro-CT point cloud is green, and the quadratic patch Lagrange patch is gold to black.

A model-based reconstruction approach was then used to improve upon the initial reconstruction, by mapping texture information across camera views to generate a dense set of corresponding 3D points on the lung surface [11]. In this case, the micro-CT surface mesh was used as a prior model to aid reconstruction of the lung surface. This involved projecting pixels from a reference camera (in this case, Camera 1) onto the quadratic Lagrange micro CT surface mesh. These points were then backprojected to another camera's sensor (in this case, Camera 2) and resampled to generate a new image, which closely resembled the real view from Camera 2. Cross-correlation techniques were then used to identify corresponding points between the resampled image and the real image from Camera 2. These corresponding points were then triangulated to generate a 3D reconstruction of the surface. This operation requires knowledge of the positions of the cameras, which were found during the camera calibration procedure.

The lung surface was reconstructed in this manner at the same inflation pressure used for fixing the lung. The motion of the lung surface during subsequent inflation pressure steps was tracked by performing 2D cross-correlation of the reconstructed corresponding points across the images acquired from each individual camera. These tracked image points were then triangulated to provide a 3D surface reconstruction at each of the inflation pressures.

3 Results

3.1 Tracking of Intrinsic Features

One of the primary concerns with reconstructing and tracking the motion of the fresh lung lobes was the lack of surface texture. To test the ability of the 2D subpixel image registration code [13] to track the intrinsic features of the fresh lung lobe, tracking was performed on a single camera view of a lung across several pressure steps, as shown in Fig 7.

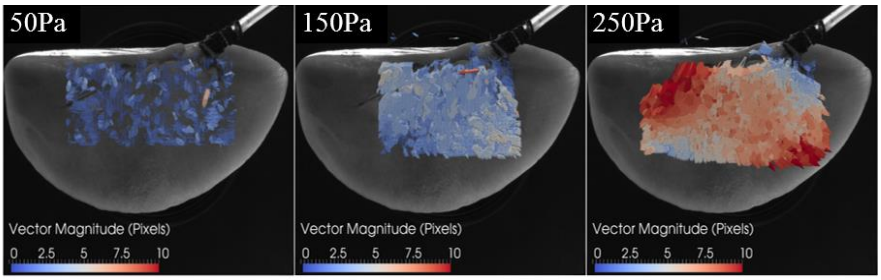

Fig 7. Single camera tracking of the intrinsic features of a left lung lobe. The pressure difference between the reference image and tracked image is shown in the top left.

Confidence thresholds [13] were set to remove points that did not have a strong correlation peak. Fig 7 illustrates that the subpixel image registration method is capable of tracking intrinsic features on the surface of the fresh lung. Failure of the

2D subpixel image registration algorithm would result in no or randomly oriented vectors being returned. The patchy, non-uniform pattern visible in Fig 7 is a result of the single camera tracking not having sufficient data to capture the displacements of the complex 3D surface of the lung.

3.1 3D Reconstruction Results

To test that reconstruction was effective on fresh lung, a region of interest (ROI) on the back of the lung, which had few specular reflections, was selected, as can be seen in Fig 8.

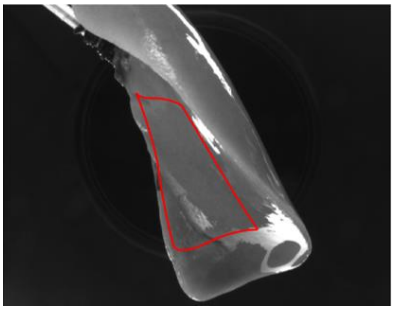

Fig 8. Region of interest for a reference camera selected on fresh lung. In the reference state the lung was inflated to 2069 Pa.

The model-based reconstruction approach described in Section 2.4 was then applied to determine corresponding points with the region of interest across the other cameras in the rig that could see the same region. For the selected ROI, two other cameras could see the same region. The resulting set of corresponding points were then triangulated to find their 3D locations, as seen in Fig 9.

The 3D locations of these points were then tracked across a range of inflation pressures. This resulted in a 3D deformation field, such as that seen in Fig 9 and Fig 10.

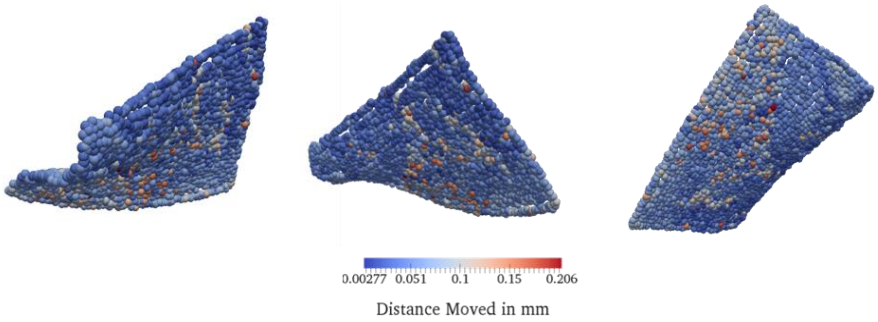

Fig 9. Reconstructed lung surface points displayed as spheres, coloured by displacement magnitude, viewed from three angles to display the surface curvature.

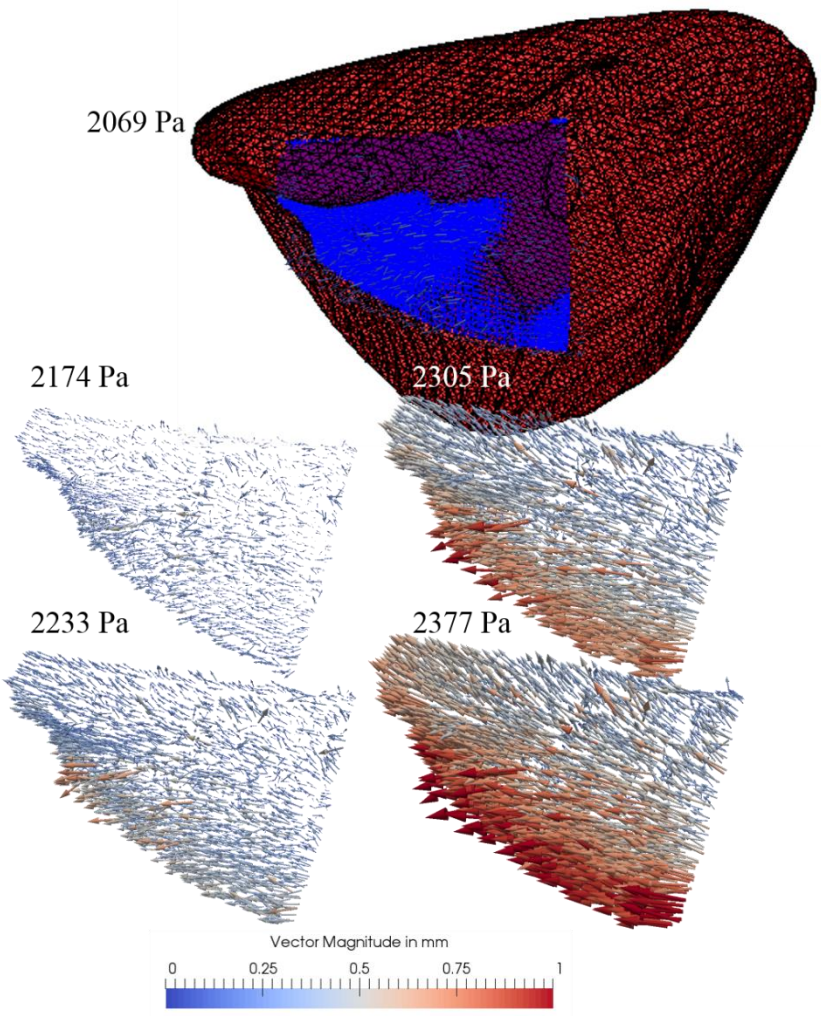

Fig 10. 3D location of the fresh lung surface tracked during inflation. The first frame is shown overlaid on the quadratic Lagrange mesh.

The 3D reconstruction of the fresh lung enabled tracking of the motion of the lung as a result of pressure increases. In this study, the fresh lung was tracked across a pressure change of 317 Pa. Over this range, the mean magnitude of the 3D motion (0.525 mm) was computed by determining the Euclidean distances between point positions at each pressure. Areas of non-uniformities in the displacement vectors are likely due failure to identify corresponding points across the three cameras. Spurious vectors could be eliminated by adjusting the cross-correlation confidence thresholds to be appropriate for 3D tracking.

4. Summary

This paper presents a pipeline for the reconstruction and tracking of the 3D motion of the *ex vivo*, intact, left lobe of a rat lung, as a result of changes in pressure. Model-based 3D reconstruction of the lungs enabled corresponding points to be found between camera views of the fresh lungs. From these, the 3D shape of a patch of the imaged lung could be determined.

The 3D reconstruction of the fresh lung patch in this study was completed with three cameras across 21 pressure steps, encompassing a total pressure change of 317 Pa. The 317 Pa pressure increase resulted in the total mean magnitude of the motion of the lung being 525.7 μm.

This study shows that the 3D reconstruction of the surface of the lungs, using only intrinsic features, is a viable approach to determine 3D shape. A prior 3D mesh was generated from a micro-CT reconstruction of a fixed lung. This mesh was aligned with sparse stereoscopic points identified using a combination of laser line identification and boundary identification on the fresh lung in the stereo-imaging rig. It was shown in this study that a combination of laser line and boundary point identification was sufficient to align the stereoscopic data with the mesh. A model-based reconstruction approach was then used to map texture information across camera views to generate a dense set of corresponding 3D points on the lung surface.

The reconstruction in this study focused on using three cameras to reconstruct a patch of the lung. This demonstrated the feasibility of using such a pipeline for the reconstruction and tracking of fresh lung tissue across a range of pressures without the need for additional surface markers.

The pipeline presented in this chapter represents the first stereoscopic imaging of *ex vivo* lungs. In addition, this work provides the first 3D tracking of the surface motion of the lungs using only intrinsic features.

As part of future work, we aim to extend the reconstruction to the whole lung, making use of all 12 cameras. This will enable 3D tracking of whole lung motion. From this, it will be possible to determine the volume change in the lung as a result of changes in pressure. This will, in turn, enable the assessment of the accuracy of the reconstruction, as volume change in the inflation system is directly measured. Future studies will apply these methods of measuring 3D deformations to identify and model the constitutive properties of the intact lung tissue.

Acknowledgments

The authors are grateful for financial support from the Royal Society of New Zealand Marsden Fund, the Medical Technologies Centre of Research Excellence, and the Auckland Bioengineering Institute.

References

[1] E. Roan and C. M. Waters, "What do we know about mechanical strain in lung alveoli?," *Am. J. Physiol. Lung Cell. Mol. Physiol.*, vol. 301, no. 5, pp. L625-35, Nov. 2011.

[2] J. C. Debes and Y. C. Fung, "Effect of temperature on the biaxial mechanics of excised lung parenchyma of the dog.," *J. Appl. Physiol.*, vol. 73, no. 3, pp. 1171–80, 1992.

[3] J. B. West, "History of respiratory mechanics prior to world war II," *Compr. Physiol.*, vol. 2, no. 1, pp. 609–619, 2012.

[4] W. Mitzner, "Mechanics of the lung in the 20th century," *Compr. Physiol.*, vol. 1, no. 4, pp. 2009–2027, 2011.

[5] L. Knudsen and M. Ochs, "The micromechanics of lung alveoli: structure and function of surfactant and tissue components The structural components for gas exchange," *Histochem. Cell Biol.*, vol. 150, pp. 661–676, 2018.

[6] J. S. Kerr, S. Y. Yu, and D. J. Riley, "Strain specific respiratory air space enlargement in aged rats," *Exp. Gerontol.*, vol. 25, no. 6, pp. 563–574, 1990.

[7] S. Richardson *et al.*, "Towards a Real-Time Full-Field Stereoscopic Imaging System for Tracking Lung Surface Deformation Under Pressure Controlled Ventilation," in *Computational Biomechanics for Medicine*, Cham: Springer International Publishing, 2019, pp. 119–130.

[8] A. HajiRassouliha, "A Toolbox for Precise and Robust Deformation Measurement," 2017.

[9] C. C. W. Hsia, D. M. Hyde, M. Ochs, E. R. Weibel, and ATS/ERS Joint Task Force on Quantitative Assessment of Lung Structure, "An Official Research Policy Statement of the American Thoracic Society/European Respiratory Society: Standards for Quantitative Assessment of Lung Structure," *Am. J. Respir. Crit. Care Med.*, vol. 181, no. 4, pp. 394–418, Feb. 2010.

[10] I. Eltoum, J. Fredenburgh, R. B. Myers, and W. E. Grizzle, "Introduction to the Theory and Practice of Fixation of Tissues," *J. Histotechnol.*, vol. 24, no. 3, pp. 173–190, 2013.

[11] T. P. Babarenda Gamage, "Constitutive parameter identifiability and the design of experiments for applications in breast biomechanics," The University of Auckland, 2016.

[12] J. Zhang, J. Hislop-Jambrich, and T. F. Besier, "Predictive statistical models of baseline variations in 3-D femoral cortex morphology," *Med. Eng. Phys.*, vol. 38, no. 5, pp. 450–457, May 2016.

[13] A. HajiRassouliha, A. J. Taberner, M. P. Nash, and P. M. F. Nielsen, "Subpixel Phase-based Image Registration Using Savitzky-Golay Differentiators in Gradient-Correlation," *Comput. Vis. Image Underst.*, vol. 170, no. 170, pp. 28–39, 2018.